FLUID FLOW AND HEAT TRANSFER CHARACTERISTICS OF A SWIRL JET IMPINGEMENT

Juliana Kuhlmann Abrantes
e-mail : kuhlmann@mec.puc-rio.br

Luís Fernando A. Azevedo
e-mail: lfaa@mec.puc-rio.br
Departamento de Engenharia Mecânica, PUC-Rio, 22453-900, Rio de Janeiro, RJ

Abstract. *The heat transfer and fluid flow characteristics of a swirl jet flow impinging on a flat plate were investigated experimentally. Jets impinging on flat surfaces have been extensively studied due to its importance as a fundamental flow and also to its wide applicability as an efficient heat transfer configuration. The present work studies the effects on the heat transfer and fluid flow patterns due to a swirl component superimposed on the axial jet flow. Instantaneous Particle Image Velocimetry(PIV) and Laser Doppler Velocimetry (LDV) measurements were performed in order to capture the axial, radial and circumferential components of the velocity field. The instantaneous velocity flow maps revealed that a vortical structure is present at the stagnation region for high values of the swirl intensity. This recirculating structure affects the local heat transfer from the jet to the plate. The study investigated the flow at Reynolds number of 21000 and a range of governing parameters given by the Swirl number and dimensionless jet-to-plate distance.*

Keywords*: Turbulence, Impinging Jet, Particle Image Velocimetry, Laser Doppler Velocimetry, heat transfer coefficients*

1. Introduction

Jets impinging on surfaces produce the highest heat and mass transfer coefficients attainable for single phase flow. For that reason, they are widely encountered in different industrial applications, such as drying of paper and fabrics, heating and cooling of metals, glass tempering, localized cooling of high power electronic components, and turbine blade cooling. Besides its practical importance, jets impinging on solid surfaces have also received considerable attention in the literature because its simple geometry presents several flow types of interest. Indeed, in the impinging jet flow configuration one finds a potential core, a stagnation zone, shear layers and developing wall jets. These are all rich flow patterns from the fundamental point of view, especially for the turbulent flow regime. Because of that, jets impinging on solid surfaces have been used to assess the predicting capabilities of computational codes and turbulence models (Cooper *et al.*, 1993).

A review of the literature shows a significant number of studies of the classical non-swirling jet impingement configuration. The papers of Martin (1977) and Downs & James (1987) review the studies conducted presenting the influence on the mass and heat transfer characteristics of a number of parameters. Among the works cited, special mention should be given to the pioneer work of Gardon and Akfirat (1965) where small heat flux gages were developed and used for measuring, for the first time, the radial variation of the Nusselt number. The peaks observed in the Nusselt number distribution were associated to turbulence intensity at the impinged wall. New computational and experimental tools have been used to reveal details of the flow field and heat/mass transfer characteristics of impinging jets. As examples of these more recent investigations, we can cite the work of Lyttle and Webb (1991), and the works of Azevedo *et al.* (1997), Fairweather & Hargrave (2002),and Geers *et al.* (2004).

The first reference to swirling impinging jets found in the literature is in the work of Martin (1977). In this review work, the author mentions that the presence of the circumferential velocity component does not produce significant changes on the heat or mass transfer from the wall. Ward and Mahmood (1982), however, presented different conclusions, indicating that the presence of the swirl flow significantly reduces the heat or mass transfer from the wall. Motivated by this contradiction in the literature, Almeida & Azevedo (1995) and Azevedo *et al.* (1997) employed the naphthalene sublimation technique to demonstrate that, in general, the presence of the circumferential velocity component acts as to decrease the average transfer coefficients as compared to the non-swirling base case. In particular, the authors verified a significant reduction of the mass transfer coefficients at the jet stagnation region. This decrease was credited to the decrease of the jet axial velocity with increasing swirl intensity. One of the most interesting results presented in these works was the identification of zones of recirculating flow at the jet stagnation region. Although only the footprints of these zones were registered by the surface visualization technique employed, the authors suggested that a toroidal vortex was present at the stagnation region.

Recently, Nozaki *et al.* (2003) combined whole field velocity and temperature measuring techniques (PIV and LIF) to investigate swirl impinging jets. The work was conducted for a relatively small value of the jet Reynolds number, namely 4000. The results obtained confirm the presence of the recirculating zone at the stagnation region, and relate the heat transfer behavior to the dynamic character of this zone.

This brief literature review demonstrated that there are still very few studies conducted on the fluid flow and heat transfer characteristics of swirl flow jet impingement. In the present work, a detailed investigation of swirl jet impingement operating in the turbulent flow regime was conducted. The flow field was characterized by both PIV and LDV techniques. Local heat transfer measurements were also obtained using the same test section employed in the fluid flow tests, which is a desirable feature that allows proper correlation of fluid flow and heat transfer results. Detailed information on the average and instantaneous behavior of the flow was obtained, which can also be used for future validation of computational models. As will be shown along the text, the presence of the circumferential component may produce significant changes on the structure of the flow with direct impact on its heat and mass transfer characteristics.

2. The experiments

The fluid flow and heat transfer measurements were conducted in the same test section presented schematically in Fig.1. Since the fluid flow measuring techniques require the use of seeding particles, the test section was designed to produce a jet flow by suction. In this way, the seeding particles could be easily ducted out of the laboratory space.

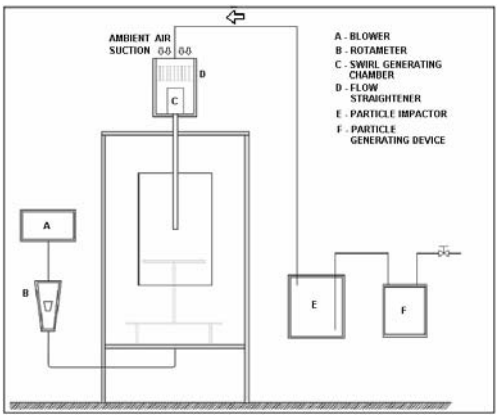

Figure 1 – Schematic view of the test section

As Fig. 1 shows, air sucked by a blower at the lower part of a large tank was forced to enter at the top of the tank forming the jet. The interior dimensions of the tank were 900 x 600 x 600 mm (height x width x depth). The air entering in the tank had to pass through a flow straightener section, through a swirl generating chamber, and through the test pipe. After leaving the test pipe, the air impinged orthogonally on a 300-mm-diameter glass flat plate. The glass plate was mounted on a telescopic support that allowed both leveling of the plate and the adjustment of the jet-to-plate distance. Two jet diameters were used: 13 and 22 mm. The swirl generating chamber was formed by a vertical thick-walled brass tube closed at its top end and open at its bottom end. At the lateral surface of this tube, eight columns of 25 holes were drilled, equally spaced circumferentially. With this geometry, air sucked by the blower penetrated tangentially in the generating chamber producing the desired swirl flow that entered into the jet pipe. Between the bottom end of the swirl generating chamber and the entrance plane of the jet pipe a swirl regulating chamber could be installed (not shown in Fig.1). This chamber was simply a set of plastic pipe spools with different lengths that could be attached to each other forming straight pipes of different lengths. By increasing the length of the pipes forming the regulating chamber one could decrease the swirl intensity. As shown in Fig. 1, the flow straightener and the swirl generating chamber were housed in a cylindrical chamber closed at the bottom, but allowing connection to the jet pipe. The top of the chamber was closed by a perforated plate that allowed the entrance of the laboratory air sucked by the blower. A 75-mm-diameter, flexible pipe was connected to a hole at the center of the perforated plate. The flexible pipe was connected to the outlet of the aerosol-generating unit used to produce the seeding particles for the flow measurements. The seeding particles used in the experiments were olive oil droplets with diameter in the 1-3 μm range. The droplets were generated by a specially designed set of four Laskin nozzles driven by compressed air from the laboratory (e.g., Raffel *et al.*, 1998 or Abrantes, 2005). After leaving the generating unit, the air stream carrying the droplets was passed through an impactor plate unit to remove the larger diameter droplets, and was finally conducted to the top of the circular chamber and into the jet. The air flow rate through the jet pipe was measured by a calibrated rotameter. The flow rate was adjusted by controlling the speed of the electrical motor that drove the blower. A frequency inverter was used for that purpose.

2.1 Velocity measurements

Two different techniques were employed to measure the fluid flow characteristics in the swirl jet impingement experiments. Instantaneous, whole field measurements were obtained by using a Particle Image Velocimetry system while point measurements of fluctuating velocity components were obtained by a laser Doppler velocimetry system. The combined use of both techniques produced valuable complementary information. Indeed, the PIV technique produces information on extensive regions of the flow, which is ideal for capturing the instantaneous nature of the flow field. However, with the measuring system employed in the experiments, the data acquisition rate was limited to 15 Hz by the pulsing frequency of the lasers. For the LDV system, data rates of up to 5 kHz are easily attainable for a particular point in the flow which is ideal for computing point flow statistics.

2.1.1 – Particle Image Velocimetry – PIV

The PIV technique is based on the measurement of the displacement of seeding particles distributed in the flow and illuminated by a planar sheet of pulsating laser light. The in-plane, two-dimensional displacement field of a small group of particles is determined by conveniently processing the images obtained. The PIV system used was manufactured by TSI Inc. The system employed a New Wave Research, 120 mJ per pulse, double-cavity laser that is able to fire double pulses at 15 Hz.

The tracer particles used were the 1-3 μm-diameter olive oil droplets already described. The CCD camera used to capture the particle images (TSI model PIVCAM 10-30) had a 1000 x 1000 pixel resolution, working at 30 frames per second. This camera was mounted on a X-Y-Z coordinate table with resolution of 0.01 mm in each direction. Synchronization between laser firing and image capturing was accomplished by a TSI model 60030 synchronizer.

A cross-correlation-based algorithm was employed to determine the particle displacement field. A recursive technique was employed to obtain high resolution vector fields by successively decreasing the interrogation window. The final displacement calculations were performed employing a 16 x 16 pixel window, with a window displacement of 8 pixels. Each instantaneous image was composed of approximately 15000 vectors.

The dimensions of the field of view were set so as to minimize bias errors in the calculation of the fluctuating velocity components. One important source of bias errors, known in the literature as pixel locking, is derived from the discrete resolution of the particle displacements when imaged by a discrete array such as a CCD sensor. These errors are minimized by setting the experiment so that an image particle occupies at least two to three pixels in the image sensor (Christensen, 2004).

When the circumferential velocity component is superimposed on the flow, the tracer particles cross the light sheet at significant velocities. In order to be able to measure the in-plane velocity components it is necessary to work with small time intervals between laser pulses, so that the particles travel a distance normal to the light sheet that it is less than its thickness. In the case of the present experiments time intervals of the order of 5 μs were used with success.

In order to obtain time-averaged fields, over 2000 images were captured and averaged. Turbulent quantities such as rms velocity fields were obtained by subtracting from each instantaneous field, the average field. In order to obtain information on the flow field away from the stagnation zone, measurements were taken by moving the coordinate table that supported the camera along the transverse direction.

2.1.2 – Laser-Doppler Velocimetry – LDV

Local, time-resolved velocity measurements were conducted employing a two-component laser Doppler velocimetry system made by TSI Inc. The system was composed of a two-color, fiber-optic-based, four-beam probe, that produced a measuring volume with dimensions of 100 x 250 μm, with a focal length of 350 mm. Both beams could be frequency shifted. The light scattered by the tracer particles were converted in electrical signal using a Color Burst and processed by an IFA 750 signal processor. Turbulent information was obtained by post-processing the data using the FIND software developed by TSI Inc. A 5W Coherent Argon-ion laser was used in the experiments. Seeding was provided by the same system already described. Typically, velocity data was acquired during 20 seconds at a rate of about 3000 samples per second. The optical probe was mounted on the same XYZ coordinate table used for the PIV experiments.

2.2 Heat transfer measurements

The test section described previously was designed to also allow the measurement of time-averaged, local heat transfer coefficients along the plate. All the test section elements employed in the fluid flow measurements were utilized in the heat transfer experiments, with the exception of the impinging plate. For the heat transfer measurements the glass plate was substituted by a 400 x 400 mm sandwich plate. The plate was formed by a 5-mm-thick Celeron plate bolted to a 12-mm-thick Plexiglas frame. Between the Celeron plate and the Plexiglas frame, a 25-mm-thick Styrene plate was inserted to minimize heat losses. The heating element was a 0.025-mm-thick Nichrome foil with dimensions of 200 x 500 mm (width x length) cemented to the Celeron plate. The edges of the foil were connected to a DC power supply, thereby producing a constant heat flux thermal boundary condition for the experiments. Seventy, 0.075-mm-diameter, Chromel-Constantan thermocouples were installed at the back surface of the heating element foil. The thermocouples were installed through holes previously drilled into the Celeron plate. A thermal conducting cement was used to secure the thermocouples in position. An alignment procedure was conducted prior to each data run to guarantee that the centerline of the jet pipe was positioned directly above the center thermocouple. A second set of thermocouples was used to verify the circumferential symmetry of the data. The readings of the thermocouples were only taken at steady state condition by an Agilent 6491 data acquisition system.

3. Data reduction procedure

The swirl jet impingement heat transfer and fluid flow are characterized by four main parameters: the jet Reynolds number, the dimensionless jet-to-plate distance and the Swirl number. The shape and turbulence intensity level of the velocity profile leaving the jet are also relevant.

The Reynolds number was evaluated directly from the volume flow measurement from the rotameter by,

$$Re = \frac{\rho U_j d}{\mu} = \frac{4\rho Q}{\pi d \mu} \tag{1}$$

where Q is the volume flow rate, ρ is the air density, d is the jet diameter, U_j is the jet exit average velocity, and μ is the air viscosity.

The swirl flow intensity is characterized by the Swirl number given by the ratio of the flow angular momentum flux, G_φ, divided by the axial linear momentum flux, G_x, multiplied by the jet radius, r. Thus,

$$S = \frac{G_\varphi}{rG_x}, \text{ with } G_\varphi = 2\pi\int \rho U W r^2 dr, \text{ and } G_x = 2\pi\rho\int U^2 r dr \quad (2)$$

where, U and W are, respectively, the time averaged axial and circumferential components of the fluid velocity measured by the LDV at the jet exit.

The local Nusselt number was evaluated by dividing the local heat flux per unit area delivered by the heating foil, q'', by the local wall-to-fluid temperature difference, $(T(r) - T_j)$, and multiplying it by the ratio of jet diameter to the air thermal conductivity, k. The heat losses by radiation from the foil surface and by conduction through the back insulation were estimated to be negligible. Thus,

$$Nu(r) = \frac{q'' d}{(T(r) - T_j)k} \quad (3)$$

Turbulent flow quantities were evaluated from the PIV and LDV data. The axial, radial and circumferential velocities are defined, for a time sample with N measurements, as the sum of the mean and fluctuating components, $U(t) = \overline{U} + u(t)$, $V(t) = \overline{V} + v(t)$ and $W(t) = \overline{W} + w(t)$ where the mean velocities were calculated from the instantaneous data as

$$\overline{U} = \sum_{i=1}^{N} \frac{U_i}{N}, \quad \overline{V} = \sum_{i=1}^{N} \frac{V_i}{N} \text{ and } \overline{W} = \sum_{i=1}^{N} \frac{W_i}{N} \quad (4)$$

The r.m.s. values of the fluctuating components and the turbulent shear stress were evaluated by

$$u' = \sqrt{\overline{u^2}} = \sqrt{\frac{1}{N}\sum_{i=1}^{N}\left(U_i - \overline{U}\right)^2}, \quad v' = \sqrt{\overline{v^2}} = \sqrt{\frac{1}{N}\sum_{i=1}^{N}\left(V_i - \overline{V}\right)^2}, \quad w' = \sqrt{\overline{w^2}} = \sqrt{\frac{1}{N}\sum_{i=1}^{N}\left(W_i - \overline{W}\right)^2}$$

$$\overline{uv} = \frac{1}{N}\sum_{i=1}^{N}(U_i - \overline{U})(V_i - \overline{V}) \quad (5)$$

4. Results and Discussion

The experimental results obtained for the flow field and local heat transfer will now be presented. Due to space limitations, only selected features will be presented, all corresponding to a Reynolds number of 21000. The complete set of experimental data, that can be found in Abrantes (2005), encompassed a parametric study involving two values of the jet-to-plate distance, (H/d = 2 and 6) and three values of the swirl intensity, given by the swirl number (S = 0, 0.3, and 0.5).

4.1. Flow field results

Figure 2 presents time-averaged and instantaneous velocity fields in the x-r plane in the vicinity of the stagnation region, obtained with the PIV technique. It allows the comparison of the non-swirl and maximum swirl cases, for H/d=2, and Re=21000. The abscissa is the dimensionless radial coordinate and the ordinate is the dimensionless vertical coordinate measured from the plate surface. Figure 2(a) shows an instantaneous velocity field for S=0, where the turbulent nature of the flow can be observed. An observation of a sequence of these figures clearly shows the periodic generation and transport of vortical structures characterizing the development of a shear layer at the jet interface. A comparison of this flow pattern with the one presented in Fig. 2(c) for S=0.5, the maximum swirl intensity investigated in the present study, shows a remarkable difference. The most striking difference is the spreading of the jet in the radial direction caused by the presence of the swirl component. Indeed, the jet is seen to practically maintain its width for the non swirl case as it develops from the jet exit plane to the impinging plate, while a significant spread is verified for S=0.5, which reflects on the displacement of the impingement point forward in the radial direction. After this point, a wall-jet-type structure is formed. The spreading of the jet causes a decrease in the levels of axial velocity in the core of the jet, leading to the formation of a second shear layer at the interface of the jet with this slow-moving-fluid region.

The severe reduction in velocity in the axial direction caused by the swirl component, combined with the adverse pressure gradient prevailing at the stagnation zone gives rise to the formation of zones of recirculating flow in the jet core. These zones of recirculating flow can be better visualized by observing the time-averaged velocity field presented in Fig. 2(d). No recirculation zone is verified for Fig. 2(b) for S=0. It should be mentioned that a large number of the vectors originally measured were suppressed from Figs. 2(b) and (d) in order not to overcrowd the figure, facilitating its interpretation.

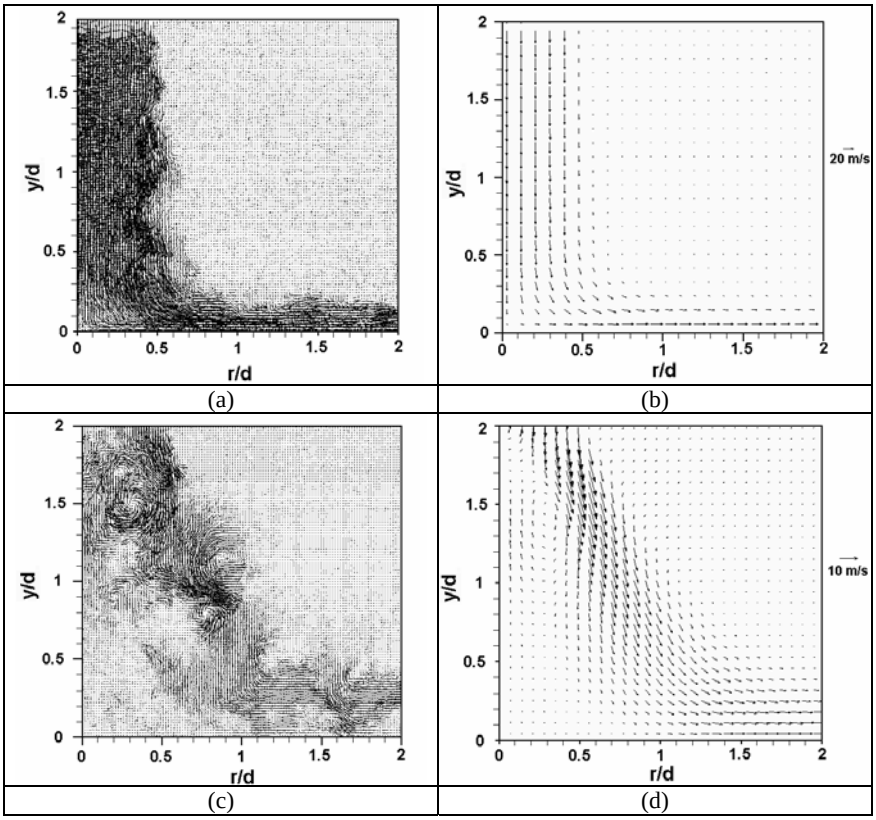

Figure 2 – Instantaneous velocity fields, *H/d*=2: (a) *S*=0; (c) *S*=0.5; Time-averaged velocity fields, *H/d*=2: (b) *S*=0; (d) *S*=0.5

Another visualization of the formation of the recirculating zones in the vicinity of the stagnation region can be seen with the aid of Fig. 3, in which contours of magnitude of the time-averaged velocity in the x-r plane are plotted. The white lines represent the projection on the x-r plane of fluid particle trajectories. For the case of *S*=0.5 depicted in Fig. 3(b), these lines can not be interpreted as streamlines due to the three dimensional nature of the mean flow field caused by the presence of the swirl flow component. The presence of two zones of recirculating flow within the jet core can be identified in Fig. 3(b). The presence of zones of recirculation in the jet core has already been documented indirectly in the experiments of Almeida et al. (1997) and more recently by Nozaki et al. (2003).

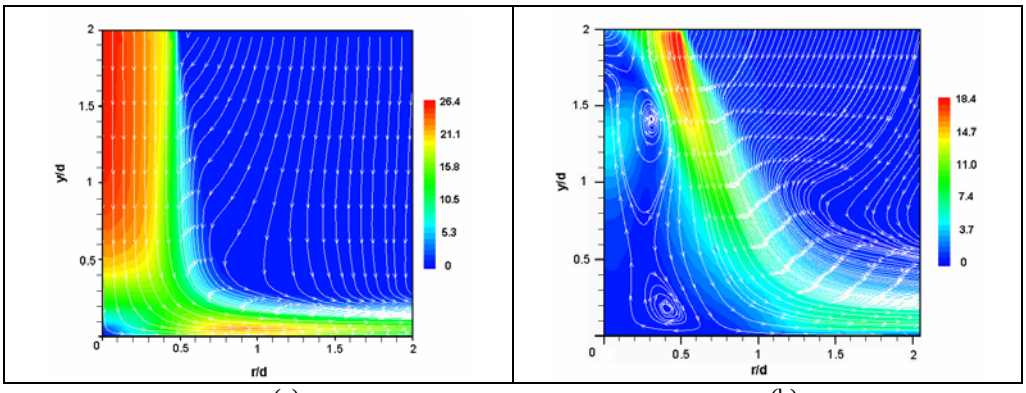

Figure 3 – Time-averaged velocity magnitude contours [m/s]; *Re*=21000, *H/d*=2; (a) *S*=0, (b) *S*=0.5

The contour maps of Figure 3 also allow us to visualize the severe deceleration suffered by the fluid as it approaches the impinging plate, in the case of no swirl. It is seen that in this case the core of the jet maintains its maximum speed up to a distance of about half diameter from the wall, from where it is decelerated to zero velocity at the wall. An examination of Figure 3(b) shows that presence of the swirl flow component not only decreases the maximum jet

velocity as compared to the non-swirl case, but also significantly reduces the velocity gradients prevailing at or near the stagnation region.

The experimental results obtained in the present work also allowed the observation of the flow characteristics as it develops in regions away from the stagnation zone, at larger values of the radial coordinate. These results were obtained by traversing the PIV camera. The velocity fields obtained were then joined to form the pictures displayed in Figures 4, 5 and 6. The figures present contours of velocity magnitude, axial and radial and turbulent velocities for the non swirl and maximum swirl cases. In all cases, the Reynolds number was 21000 and the dimensionless jet-to-plate distance was equal to 2. The contours of velocity magnitude presented in Figure 4(a) and (b) show that, apart from the significant differences in the stagnation region already commented, there are no major changes in the development of the wall jet caused by the presence of the swirl component. This is probably due to the rapid decay of the circumferential velocity with the radial coordinate.

Figures 5(a) and (b) present the contours of axial turbulent rms velocity, in which it can be verified that for both, the swirl and non swirl cases, the region of larger intensity is located downstream of the pipe jet wall. The intensity of the axial turbulent velocity is, however, higher for the swirl case probably due to double shear layer developing there, as already mentioned in the comments regarding the results of Figure 2. For the rest of the field, the presence of the wall seems to dump the axial turbulent velocity in a similar way for the swirl and non swirl cases.

In the case of the radial turbulent rms velocity, the results presented in Figure 6(a) and (b) demonstrate that, while the peak intensity for the swirl case is still located at the wake of the jet pipe wall, in the non swirl case the maximum radial turbulent velocity intensity is found at the initial developing stages of the wall jet, indicating a peak of turbulence intensity at that location.

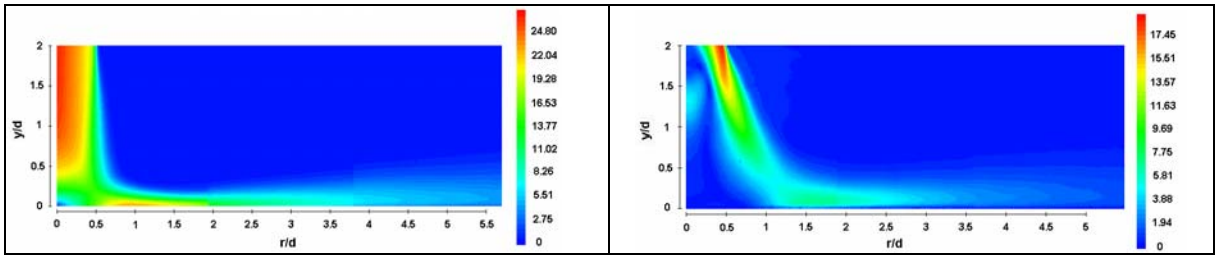

(a) (b)

Figure 4 – Time-averaged velocity magnitude contours, $\sqrt{\overline{U}^2 + \overline{V}^2}$, [m/s]. *Re*=21000, *H/d*=2. (a) *S*=0. (b) *S*=0.5

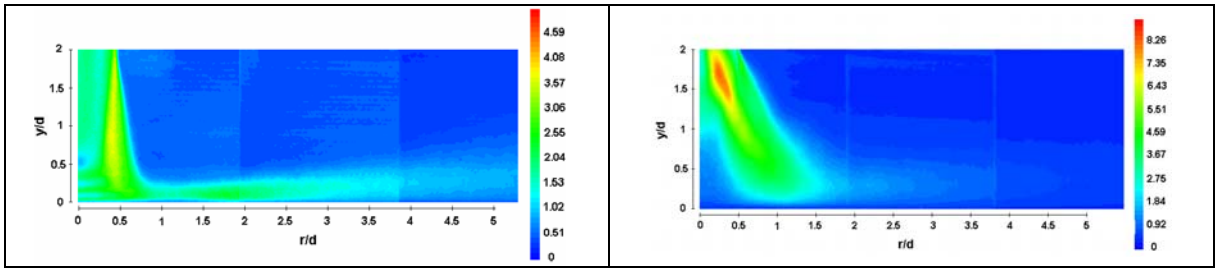

(a) (b)

Figure 5 – Axial turbulent rms velocity contours - **u'** [m/s]. *Re*=21000, *H/d*=2. (a) *S*=0; (b) *S*=0.5

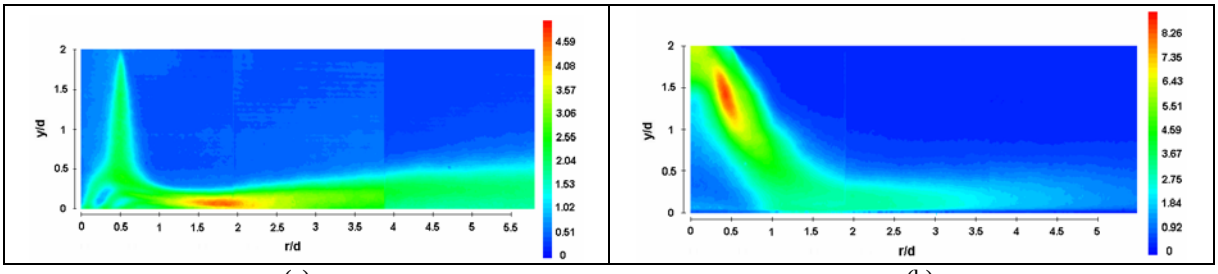

(a) (b)

Figure 6 – Radial turbulent rms velocity contours - **v'** [m/s]. *Re*=21000, *H/d*=2. (a) *S*=0; (b) *S*=0.5

Figures 7(a) and (b) were prepared to convey a better quantitative comparison of the turbulent velocities for the swirl and no swirl cases. Figure 7(a) shows the axial and radial turbulent dimensionless rms velocities for the no swirl case while Fig. 7(b) displays the same information for *S*=0.5. Figure 7(b) also includes data on the turbulent velocity in the circumferential

direction measured with the LDV system. All these values presented in figure 7 were measured at a vertical coordinate very close to the plate surface, namely, y = 0.02d. Results of turbulence intensity close to the wall are relevant to help understand the heat transfer characteristics of the jet impingement configuration.

The results of Figure 7 show that, as expected, the radial component of the turbulent velocity for the swirl and no swirl cases is higher than the axial component, damped by the wall at this vertical coordinates. Also, the peaks in the radial component are of similar magnitude regardless of the presence of the swirl component. The turbulent circumferential velocity is seen to be of the same order of magnitude as the radial component, although it appears to reach its maxima and start decaying at a smaller radial distance. Since the three components of the turbulent velocity were measured for the swirl case, it was possible to compute the turbulent kinetic energy distribution along the radial coordinate for that particular vertical coordinate. The turbulent kinetic energy was calculated by $k=(u'^2+v'^2+w'^2)/2$, and its presented in Figure 7(b) in dimensionless form. U_j is the jet mean exit velocity.

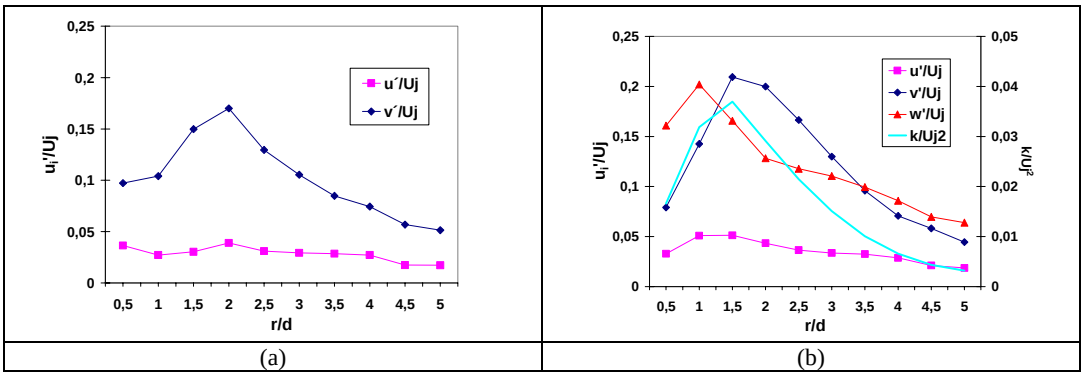

Figure 7 – Profiles of rms velocities and turbulent kinetic energy at y = 0.02d. H/d = 2; *(a)* S=0; (b) S=0.5.

4.2. Effects of the flow field structure on local heat transfer

We now present the results obtained for the local heat transfer from the impinging plate. The results shown in Fig. 8 include data for configurations that did not have their flow characteristics presented in the present paper due to space limitations. These are the jet-to-plate distance, H/d=6, and the intermediate swirl intensity given by S=0.3. In the radial profiles of local Nusselt number presented as a function of the dimensionless radial coordinate, the open symbols represent the results for H/d=6, while the solid symbols are keyed to H/d=2.

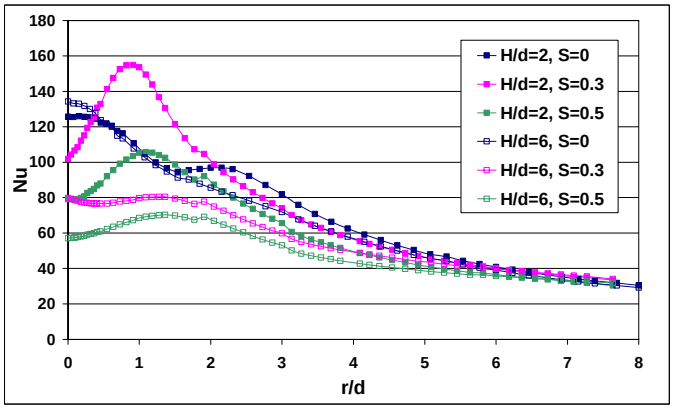

Figure 8 – Radial distribution of the local Nusselt number, Re=21000. Solid symbols: H/d=2, open symbols: H/d=6.

Starting with the analysis of the non-swirling cases, it can be seen that the local Nusselt number peaks at the stagnation point for H/d=6, decreasing monotonically with the radial coordinate. As the jet-to-plate distance is decreased to H/d=2 the maximum stagnation number is still at the stagnation point, but it is somewhat lower than the value measured for H/d=6. A secondary maxima in the Nu distribution is found around r/d=2. From that point on, a monotonic decrease is observed and the Nu values tend to the same asymptotic value found for H/d=6. A plausible explanation for the higher value of Nu at stagnation for H/d=6 concerns the turbulence generated mostly in the axial direction near the jet pipe wall and in the shear layer that is formed thereafter. For H/d=6, the mixing layer diffuses inward reaching the jet centerline, thereby raising the levels of turbulence intensity at the stagnation region. When the jet-to-plate distance is shortened to H/d=2, the interaction between the free shear layer and the jet core is attenuated, that is, this process is interrupted by the presence of the plate. As for the

secondary peak in the Nusselt number distribution for H/d=2, it can be associated with the region where the radial turbulence intensity is higher. This can be seen in Figures 6(a) and 7(a). The behavior of the Nu distribution just described for the non swirl case is in good agreement with the literature (e.g., Lyttle & Webb, 1992).

The introduction of a circumferential velocity component on the jet flow is seen to significantly decrease the local Nu at stagnation. Indeed, in Figure 8 one can verify a decrease of about 40% when the swirl number is increased from 0 to 0.5, for H/d=2. For H/d=6 the magnitude of the decrease reaches 60%. This decay in Nu at stagnation can be associated with the weakening of the axial velocity due to the formation of zones of recirculating flow at the stagnation region presented previously, and also with the lower values of turbulence intensity in this region. The Nu distribution for H/d=6 which is monotonic for S=0, displays points of maxima when the swirl component is present. The positions of these maxima coincide with peaks in turbulence intensities measured, but not shown in the present paper. For the case of H/d=2, the Nu distributions present much more pronounced maxima. For S=0.3, for instance, the peak value located at about r/d=1, reaches a value that is 25% higher than the stagnation Nu for the no swirl case, meaning that swirl can indeed enhance heat transfer at particular radial locations. The location of the maxima, for both swirl intensities, agrees with the measured peaks in turbulence intensity, as can be seen in Figure 7(b), for S=0.5.

An interesting observation that can be made from Figure 7 is the fact that the presence of swirl can locally raise the heat transfer substancially, and this local peak possibly reaches a maximum value around S=0.3. Due to limitations in the test section design, it was not possible to vary continuously the value of S in order to search for the exact swirl value that maximizes local heat transfer for a particular jet-to-plate distance. A verification of the quantitative data obtained from the flow measurements indicates that, while the time-averaged radial velocity component close to the wall at the location of the peak heat transfer (r/d=1) is about $0.9U_j$ (U_j is the jet average velocity) when S=0, it decreases to $0.3U_j$ and $0.15U_j$ when the swirl number is increased, respectively, to 0.3 and 0.5. The rms radial turbulent velocity close to the wall however, peaks at S=0.3. It is 0.1 U_j for S=0, $0.25U_j$ for S=0.3, and $0.15U_j$ for S=0.5. Apparently the two opposing effects – lower average radial velocity and higher radial rms turbulent velocity – combine to maximize the heat transfer from the wall at r/d=1 when S=0.3. Further investigation is necessary to clarify this issue.

5. Conclusions

The present work studied the fluid flow and heat transfer characteristics of a swirl jet impingent configuration. The parameters investigated were the jet Reynolds number, the dimensionless jet-to-plate distance, and the intensity of the swirl flow given by the swirl number.

Instantaneous and time-averaged velocity field measurements obtained by PIV and LDV techniques produced detailed data on the mean and turbulent characteristics of the flow. Heat transfer measurements performed in the same test section produced local distributions of the Nusselt number. The results revealed that the presence of a swirl velocity component generates recirculation zones in the stagnation region which significantly reduce the stagnation Nusselt numbers. Peaks in the Nusselt distribution were observed in the swirl jet configuration that were linked to peaks in the turbulent velocities close to the wall.

The experimental work conducted gathered detailed data on the flow field and local heat transfer that is available to be used in the validation of turbulent heat transfer and fluid flow computational models.

4. References

Almeida, J.A., Azevedo, L. F. A., “Flow Visualization Study of Swirling Jet Impingement”, XIII Congresso Brasileiro de Engenharia Mecânica, Belo Horizonte, MG, 1995 (CD-ROM).

Christensen, K.T., “The Influence of Peak-Locking Errors on Turbulence Statistics computed from PIV Ensembles”, Experiments in Fluids, 2004, vol.36, pp 484 – 497.

Cooper, D., Jackson, D.C., Launder, B. E., Liao, G. X., “Impinging Jet Studies for Turbulence Model Assessment – I. Flow Field Experiments”, International Journal of Heat and Mass Transfer, 1993, vol. 36, No. 10, pp 2675 – 2684.

Downs, S.J., James, E.H., “Jet Impingement Heat Transfer – A Literature Survey”, ASME Paper No 87 – HT – 35, ASME, 1987.

Gardon, R., Akfirat, J.C., “The Role of Turbulence in Determining the Heat Transfer Characteristics of Impinging Jets”, International Journal of Heat and Mass Transfer, 1965, vol.8, pp 1261 – 1272.

Gears, L. F. G., Tummers, Hanjalic, K., “Experimental Investigation of Impinging Jet Arrays”, Experiments in Fluids, 2004, 36, pp 946 – 958.

Lyttle, D., Webb, B.W., “Secondary Heat Transfer Maxima for Air Jet Impingement at Low Nozzle-to-Plate Spacings”, 2nd World Conference on Experimental Heat Transfer, Fluid Mechanics and Thermodynamics, Iugoslávia, 1991, pp. 776 – 783.

Martin, H., “Heat and Mass Transfer Between Impinging Gas Jets and Solid Surfaces”, Advances in Heat Transfer, 1977, pp 1-60.

Nozaki, A., Igarashi, Y. e Hishida, K., “Heat Transfer Mechanism of a Swirling Impinging Jet in a Stagnation Region”, Heat Transfer – Asian Research, 2003, vol. 32, No. 8.

Raffel M., Willert C., Kompenhans J., “Particle Image Velocimetry – A Practical Guide”
Ed. Springer.

Ward, J., Mahmood, M., “Heat Transfer from a Turbulent, Swirling, Impinging Jet”, 7th Int. Heat Transfer Conference, 1982, pp 401 – 408.